SIRIUS STORAGE RING EMITTANCE MEASUREMENT USING UNDULATOR RADIATION

J. B. Vieira[2*], G. R. Ascenção[2], S. A. L. Luiz
Brazilian Synchrotron Light Laboratory - LNLS, Campinas - SP, Brazil
[2]also at Gleb Wataghin Institute of Physics, University of Campinas, Campinas - SP, Brazil

Abstract

This work presents a measurement the SIRIUS electron-beam emittance from undulator radiation at EMA and MANACA beamlines. Two observables are used: the peak-to-valley ratio of the projected even-harmonic profile and the direct minimization of the 2D spatial distribution intensity versus radiation energy. The two beamlines provide distinct beta functions, which helps separate emittance from optics. Turn-by-turn (TbT) beta-beating sets the beta uncertainty, and the undulator field maps are corrected to align measured and simulated resonances. The extracted emittances are consistent with the expected ~ 250 pm.rad value.

INTRODUCTION

Low-emittance storage rings demand beam diagnostics that remain sensitive in the picometer-radian regime. At SIRIUS, standard imaging becomes less robust when the photon-beam size approaches detector resolution and the diffraction limit [1].

This work uses undulator radiation from two beamlines with different optics: EMA, a low beta straight section [2], and MANACA, a high beta straight section [3]. The analysis combines SPECTRA-based simulations, field-map calibration, and spatial-profile fitting [4, 5].

The paper is organized as follows: first, the model and objective functions are defined, then a brief introduction of the beamlines and methods is given, and finally, the fitted parameters and extracted emittance values are shown.

Table 1: SIRIUS storage ring and insertion-device parameters used in the emittance study.

Storage ring parameters	Value		Symbols [units]
Nominal energy	3.0		E_0 [GeV]
Natural emittance	250		ϵ_0 [pm rad]
Coupling (emittance ratio)	1		κ [%]
Energy spread	0.084		σ_E [%]
	EMA	MNC	
Hor. beta function @ ID SS center	1.499	17.22	β_x [m]
Ver. beta function @ ID SS center	1.435	3.60	β_y [m]
Undulators parameters	IVU	APU	
Period	18.5	22.0	λ_u [mm]
ID length	2.0	1.2	L [m]
No. periods	108	51	
Máx. deflection parameter	2.14	1.47	

The adopted strategy combines simulations performed with SPECTRA and measured two-dimensional photon images. The analysis focuses on two observables only: the peak-to-valley ratio of the projected even-harmonic profile, and the direct minimization of the spatial distribution as a function of radiation energy.

* jefferson.vieira@lnls.br

THEORETICAL APPROACH

The size of the electron beam propagated at a distance d [5] follows:

$$\sigma_e^2 = \underbrace{\epsilon\beta_0 + \epsilon\left(-2\alpha_0 d + \frac{1+\alpha_0^2}{\beta_0}d^2\right)}_{\approx 10^{-8}} + \underbrace{\sigma_\delta^2\eta_0^2}_{\approx 10^{-16}} + \underbrace{\sigma_\delta^2\eta_0'^2 d^2}_{\approx 10^{-18}}, \quad (1)$$

where ϵ is the emittance, d is the propagation distance, and η_0, η_0' are the dispersion terms in the SIRIUS straight sections.

The source-point dispersion is negligible in both beamlines, so the energy-spread term is much smaller than the emittance term for the propagation distances used here. The orders of magnitude of the terms involved are expressed in equation 1. The dispersive term within the undulator was calculated using the symplectic integrator [6]. This reduces the fit to ϵ and $\beta_{x,y}$, with the remaining degeneracy handled by combining fits from EMA and MANACA. So the fit is dominated by the emittance–beta dependence.

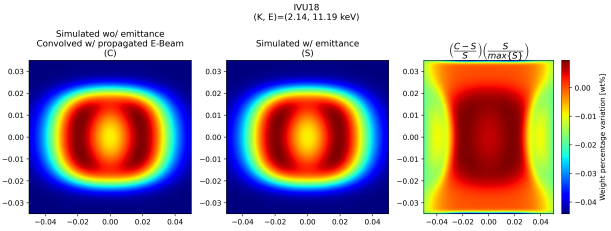

Figure 1: Comparison between direct emittance-dependent flux calculation and FFT-based convolution. The small difference validates our approach.

The photon distribution from a single electron is convolved with the propagated electron distribution using FFT-based numerical convolution [7]. This keeps the SPECTRA [8] calculation fast while preserving the flux distribution, as one can see in Figure 1.

BEAMLINE SETUP

EMA uses the In-Vacumm Undulator (IVU18) source (Table 1), with Photon Beam Visualization (DVF) at 33.35 m, DVF is a scintillator-based imaging system of Yttrium Aluminum Garnet (YAG) material. The Double-Crystal Monochromator (DCM) was scanned in ~10 eV steps across

the selected harmonics. MANACA, on the other hand, uses the Adjustable Phase Undulator (APU22) source (Table 1), with DVF at 30.16 m from the source. The same DCM scan strategy was used, with the slits opened to maximum acceptance. The beamline setup can be seen in Figure 2 and 3.

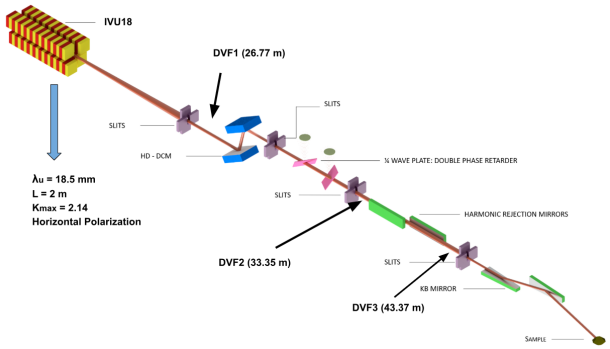

Figure 2: EMA optics layout with the IVU18 source and the DVF2 detector position.

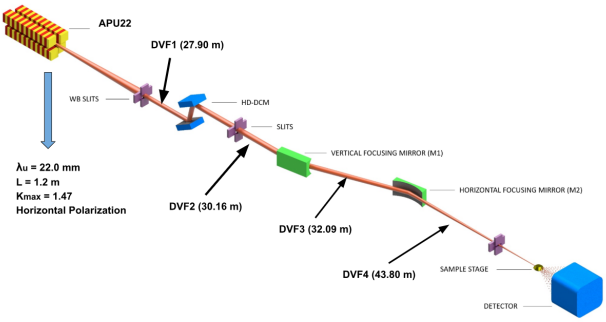

Figure 3: MANACA optics layout with the APU22 source and the DVF2 detector position.

EXPERIMENTAL MEASUREMENTS

Due to the degeneracy between beta and emittance, it is necessary to know the uncertainty of beta in order to calculate the expected value of the emittance. Therefore, beta-beating measurements were performed, as shown in Figure 4.

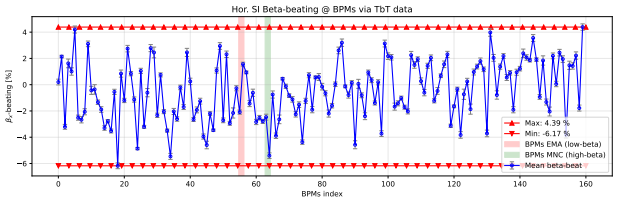

Figure 4: Horizontal beta beating from turn-by-turn data. The BPM spread defines the beta uncertainty used in the fits.

Turn-by-turn optics measurements give a horizontal beta-beating range of +4.39% to −6.17%. We use ±6% as the measured uncertainty and ±10% as a conservative envelope.

EMA data were taken with the IVU18 at 4.4 mm gap and MANACA was measured with the APU22 at 2 mm phase, undulators conditions that have a measured magnetic field. Figure 5 shows a set of measurements from EMA beamline.

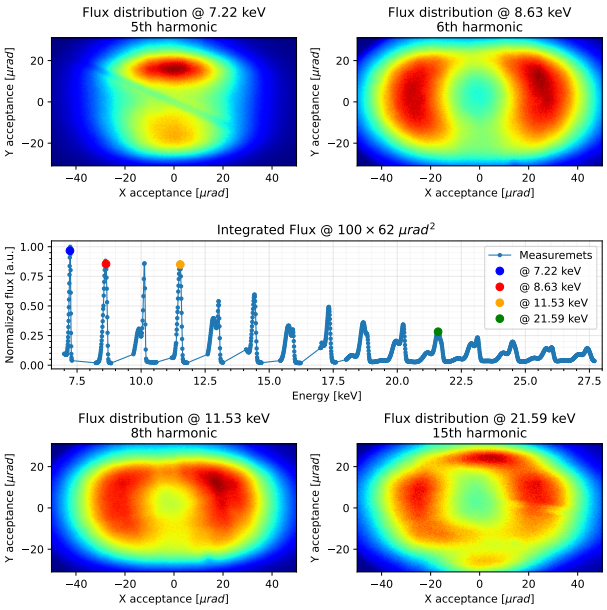

Figure 5: EMA measured flux distributions for nominal conditions.

RESULTS

Field Measurement Adjust

The EMA spectrum showed a resonance mismatch with the IVU18 field map. A correction $\Delta B_{\text{eff}}/B_{\text{eff}} = 0.16\%$, or $\Delta B_{\text{eff}} = -21$ G was necessary. After this correction, the simulated and measured resonances aligned and the field model became usable for the fit [9]. For MANACA, the APU22 field map also required correction. A uniform effective-field change of 0.15%, or $\Delta B_{\text{eff}} = 10$ G, aligned the harmonic peaks and improved the spectral agreement. Figure 6 shows the result of this adjustment in the magnetic field measurement.

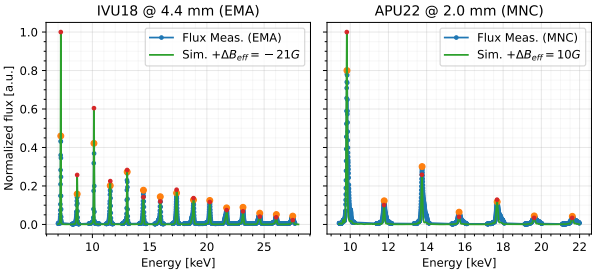

Figure 6: Measured flux at an aperture of 20 x 20 $urad^2$ for the EMA and MANACA beamlines (blue line). Simulated flux with IVU and APU field measurement adjust in the same aperture (green line). The simulation included YAG absorption and DCM reflectivity. The corrected field aligns the simulated and measured resonance energies.

Emittance Fitting

The peak-to-valley objective function gives nominal emittances of about 264 pm.rad. With ±10% beta uncertainty, the EMA uncertainty is about ±25 pm.rad. The MANACA fit gives $\langle \epsilon \rangle$ = 261 pm.rad with an uncertainty of ±15 pm.rad. These results are shown in Figure 7.

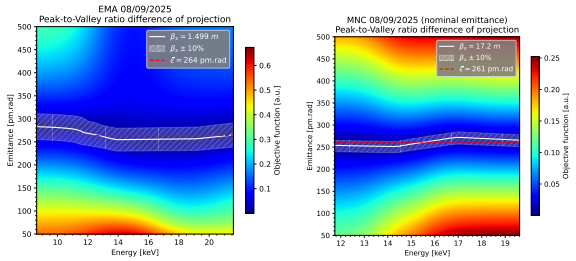

Figure 7: EMA and MANACA emittance fit from the peak-to-valley objective function. The high-β optics reduce the beta-induced spread of the solution.

For spatial-profile minimization, the Nelder-Mead numerical method was used [10]. The parameters varied during minimization were emittance, rotation, and translation of the simulated spatial-profile. Figure 8 shows the result of the spatial-profile minimization for the EMA beamline for measurements taken on two different days.

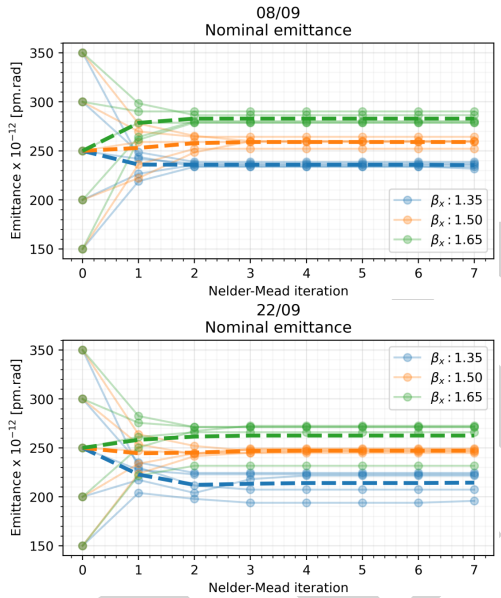

Figure 8: EMA emittance fit from the spatial-profile minimization objective function.

The reduced sensitivity at MANACA beamline follows from the comparable values of β_x and the 30.16 m propagation distance, which weakens the beta sensitivity. his loss of sensitivity becomes clear when the analysis of the emittance derivative of the equation 1 is performed:

$$\frac{\partial \epsilon}{\partial \beta} = \sigma^2 \frac{d^2 - \beta^2}{(d^2 + \beta^2)^2} = \begin{cases} \frac{\sigma^2}{d^2} & , \text{when } \beta \ll d \\ 0 & , \text{when } \beta = d \\ -\frac{\sigma^2}{\beta^2} & , \text{when } \beta \gg d \end{cases} \quad (2)$$

where σ is the font size that generates the measured image, which is fixed.

Figure 9 shows the sensitivity of emittance as a function of the beta value. It is noteworthy that at large distances, where the spatial profile is being measured, and for small beta, the emittance uncertainty is greater given a beta uncertainty.

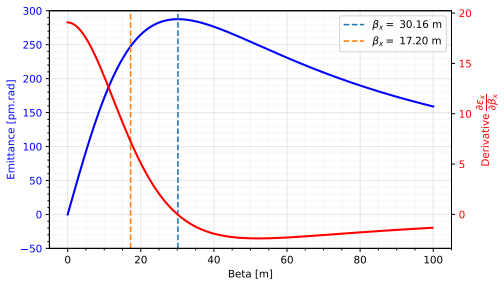

Figure 9: Emittance sensitivity as a function of beta value.

CONCLUSION

The SIRIUS emittance was extracted from undulator radiation at EMA and MANACA using two observables: projected even-harmonic peak-to-valley ratios and 2D spatial-profile minimization. The calibrated field maps and turn-by-turn beta beating are used to estimate the uncertainty of the emittance measurements.

The nominal values are consistent across beamlines: ~ 264 ± 25 pm.rad at EMA and 261 ± 15 pm.rad at MANACA. EMA is more sensitive but more beta-dependent; MANACA is less sensitive but more stable. Together, they provide consistent emittance estimatives.

ACKNOWLEDGEMENTS

The authors thank the SIRIUS Accelerator Physics Group and the Insertion Devices and Photon Diagnostics Group for their support during the machine studies.

REFERENCES

[1] N. Samadi, X. Shi, L. Dallin, and D. Chapman, "Source size measurement options for low-emittance light sources," *Phys. Rev. Accel. Beams*, vol. 23, p. 024801, 2020. doi:10.1103/PhysRevAccelBeams.23.024801

[2] EMA beamline, https://lnls.cnpem.br/facilities/ema-en/.

[3] MANACÁ beamline, https://lnls.cnpem.br/facilities/manaca-en/.

[4] T. Tanaka, "Major upgrade of the synchrotron radiation calculation code SPECTRA," *J. Synchrotron Radiat.*, vol. 28, pp. 1267–1272, 2021. doi:10.1107/S1600577521004100

[5] T. Tanaka and H. Kitamura, "SPECTRA: a synchrotron radiation calculation code," *J. Synchrotron Radiat.*, vol. 8, pp. 1221–1228, 2001. doi:10.1107/S090904950101425X

[6] G. R. Ascenção *et al.*, "Symplectic integrator for insertion devices tracking at SIRIUS", presented at the IPAC'26,

Deauville, France, May 2026, paper THP5320, this conference.

[7] J. W. Cooley and J. W. Tukey, "An algorithm for the machine calculation of complex Fourier series," *Math. Comp.*, vol. 19, pp. 297–301, 1965. doi:10.2307/2003354

[8] T. Tanaka, "Numerical methods for characterization of synchrotron radiation based on the Wigner function method," *Phys. Rev. Spec. Top. Accel. Beams*, vol. 17, p. 060702, 2014. doi:10.1103/PhysRevSTAB.17.060702

[9] J. A. Clarke, *The Science and Technology of Undulators and Wigglers*, vol. 4, Oxford University Press, 2004. doi:10.1093/acprof:oso/9780198508557.001.0001

[10] F. Gao and L. Han, "Implementing the Nelder-Mead simplex algorithm with adaptive parameters," *Comput. Optim. Appl.*, vol. 51, pp. 259–277, 2012. doi:10.1007/s10589-010-9329-3